Regional and Temporal Differences in Gene Expression of $LH_{BETA}T_{AG}$ Retinoblastoma Tumors

Samuel K. Houston,[1] *Yolanda Pina,*[1] *Jennifer Clarke,*[2] *Tulay Koru-Sengul,*[2] *William K. Scott,*[3] *Lubov Nathanson,*[3] *Amy C. Schefler,*[1] *and Timothy G. Murray*[1]

Purpose. The purpose of this study was to evaluate by microarray the hypothesis that $LH_{BETA}T_{AG}$ retinoblastoma tumors exhibit regional and temporal variations in gene expression.

Methods. $LH_{BETA}T_{AG}$ mice aged 12, 16, and 20 weeks were euthanatized ($n = 9$). Specimens were taken from five tumor areas (apex, anterior lateral, center, base, and posterior lateral). Samples were hybridized to gene microarrays. The data were preprocessed and analyzed, and genes with a $P < 0.01$, according to the ANOVA models, and a $\log_2$-fold change >2.5 were considered to be differentially expressed. Differentially expressed genes were analyzed for overlap with known networks by using pathway analysis tools.

Results. There were significant temporal ($P < 10^{-8}$) and regional differences in gene expression for $LH_{BETA}T_{AG}$ retinoblastoma tumors. At $P < 0.01$ and $\log_2$-fold change >2.5, there were significant changes in gene expression of 190 genes apically, 84 genes anterolaterally, 126 genes posteriorly, 56 genes centrally, and 134 genes at the base. Differentially expressed genes overlapped with known networks, with significant involvement in regulation of cellular proliferation and growth, response to oxygen levels and hypoxia, regulation of cellular processes, cellular signaling cascades, and angiogenesis.

Conclusions. There are significant temporal and regional variations in the $LH_{BETA}T_{AG}$ retinoblastoma model. Differentially expressed genes overlap with key pathways that may play pivotal roles in murine retinoblastoma development. These findings suggest the mechanisms involved in tumor growth and progression in murine retinoblastoma tumors and identify pathways for analysis at a functional level, to determine significance in human retinoblastoma. Microarray analysis of $LH_{BETA}T_{AG}$ retinal tumors showed significant regional and temporal variations in gene expression, including dysregulation of genes involved in hypoxic responses and angiogenesis. (*Invest Ophthalmol Vis Sci.* 2011;52:5359–5368) DOI:10.1167/iovs.10-6321

From the [1]Bascom Palmer Eye Institute, the [2]Division of Biostatistics, Department of Epidemiology and Public Health, and the [3]Department of Molecular Genomics, University of Miami, Miami, Florida

Supported by National Institutes of Health center Grants R01 EY013629, R01 EY12651, and P30 EY014801; the American Cancer Society, Sylvester Comprehensive Cancer Center; and an unrestricted grant to the University of Miami from Research to Prevent Blindness, Inc.

Submitted for publication August 1, 2010; revised December 16, 2010, and March 20 and April 19, 2011; accepted April 20, 2011.

Disclosure: **S.K. Houston**, None; **Y. Pina**, None; **J. Clarke**, None; **T. Koru-Sengul**, None; **W.K. Scott**, None; **L. Nathanson**, None; **A.C. Schefler**, None; **T.G. Murray**, None

Corresponding author: Timothy G. Murray, Bascom Palmer Eye Institute, P.O. Box 016880, Miami, FL 33101; tmurray@med.miami.edu.

Retinoblastoma (RB) is the most common intraocular malignancy in children, affecting approximately 1 in 15,000, for an incidence of 250 to 300 new diagnoses a year in the United States.[1–4] As treatment has progressed from external beam radiation therapy (EBRT) to chemoreduction combined with focal therapies, survival rates have climbed to 99% with a large percentage of children maintaining vision.[5] Despite the significant advancements in treatment and survival, current chemotherapy regimens and focal therapies may result in complications. Children are subjected to toxic chemotherapeutic drugs for multiple cycles, resulting in considerable risk for systemic toxicities.[6–8] Focal consolidation therapies also contribute to morbidity, depending on the intraocular tumor size and location.[9] Finally, chemoreduction success varies depending on tumor classification, with more advanced eyes achieving tumor control in 47% to 83% of cases.[10,11] As a result, a greater understanding of tumorigenesis is necessary to develop adjuvant therapies to potentially treat tumors that are unresponsive to current treatment protocols and to minimize local and systemic complications of treatment.

The genetics of RB development have been studied, beginning with Knudson's "two hit" hypothesis.[12] In RB development, mutations or epigenetic changes in both alleles of the *RB1* gene lead to loss of retinoblastoma protein (pRB). pRB binds to E2F, which acts as a transcriptional regulator of the cell cycle. Loss of both *RB1* alleles leads to susceptibility of retinal cells to formation of RB. It has been proposed that development of RB requires more than the two hits proposed by Knudson, with Corsen and Gallie[13] reviewing the literature for evidence of further genetic changes necessary for tumor development.

The paradigm of cancer treatment and understanding has shifted from solely targeting hyperproliferative tumor cells and associated oncogenes/tumor suppressor genes to also targeting cancer stromal tissue, which consists of complex multicellular interactions, termed the tumor microenvironment.[14,15] This environment consists of a plethora of cell types, including endothelial cells, fibroblasts, and inflammatory cells,[16] that, along with numerous growth factors and signaling molecules, contribute to tumorigenesis. Hypoxia has been strongly correlated with tumor growth, progression, resistance to therapy, and metastasis.[17] It has been shown that through O^2-sensitive pathways, hypoxia alters tumor cell behavior, resulting in an integrated response of tumor cells to the tumor microenvironment, leading to altered gene expression and tumor adaptation and survival. Alterations to hypoxia include signaling through the mammalian target of rapamycin (mTOR), hypoxia inducible factor (HIF), and the unfolded protein response (UPR). These responses lead to altered cellular metabolism, angiogenesis, and other cell survival mechanisms.[18] The genetic changes associated with a tumor's adaptation to the microenvironment are prospective avenues for more specific and targeted therapy. In addition, an understanding of the timing of

gene expression is fundamental in the optimal use of novel, multimodal adjuvant treatments.

Hypoxia and angiogenesis have been shown to be significantly associated with tumor proliferation and metastasis. Our previous studies with the $LH_{BETA}T_{AG}$ mouse model of RB have shown that 20% to 26% of tumoral areas are hypoxic and that there is a spatial difference, with hypoxia primarily in the central and basal regions of the tumor.[19] In addition, we have shown that there is a spatial distribution of blood vessel maturation, with mature blood vessels concentrated centrally, while immature neovessels radiate peripherally. As a result, we have proposed that RB tumors grow radially from the center, with the apex, anterior, and posterior margins serving as the leading edges.[20]

We hypothesize that there are regional and temporal differences in gene expression of murine RB tumors corresponding to areas of tumor heterogeneity and variations in tumor microenvironment. These variations may provide valuable information regarding specific genes and pathways that facilitate tumor growth, progression, and resistance to treatment. The purpose of our study was to evaluate these regional and temporal differences by using mRNA microarray analysis in a transgenic model of RB.

Methods

$LH_{BETA}T_{AG}$ Mouse Model for RB

The study protocol was approved by the University of Miami Institutional Animal Care and Use Review Board Committee. The $LH_{BETA}T_{AG}$ transgenic mouse model used in this study has been characterized previously.[21] This animal model develops bilateral multifocal retinal tumors that are stable and grow at a predictable rate (i.e., tumor at 4 weeks is grossly undetectable, at 8 weeks is small, at 12 weeks is medium, and at 16 weeks is large), with histopathologic, immunopathologic, and ultrastructural features that resemble human RB tumors. The $LH_{BETA}T_{AG}$ mouse model has contributed to elucidating mechanisms in tumor development and progression and to providing a platform for the development of adjuvant therapies.

Molecular Genomic Array Analysis in $LH_{BETA}T_{AG}$ Retinal Tumor Growth

Transgenic mice with documented intraocular tumors were killed and the eyes enucleated at 12, 16, and 20 weeks of age ($n = 9$; three at each time point). These time points were chosen to represent early to advanced tumors and to correspond to time points studied in this model regarding angiogenesis, hypoxia, gelatinase expression, and tumor response to therapy. Five 3.37-mm^3 sections were obtained from each tumor (apex, anterior lateral, center, base, and posterior lateral). Samples were meticulously dissected under a microscope by an experienced handler. With the time points chosen (12, 16, and 20 weeks), tumors had already grown to a macroscopic size, allowing an experienced handler to dissect them without obtaining normal retina, as the tumor has already expanded into the globe with boundaries distinct from normal retina. Although there is always a possibility of contamination, dissection protocols were meticulously used in ascertaining the extraction of sufficient and appropriate samples. Samples were obtained from the five areas based on the proposed mechanism of tumor growth and progression, with radial growth from the center. Leading edges have been shown to consist of more immature vasculature, whereas, central areas consisted of mature vasculature as well as a higher percentage of hypoxia.[19,22] All specimens ($n = 45$) were placed in a lysis solution and stored at −20°C until analyzed. The samples were hybridized (16 hours) to a unique gene microarray chip that provides whole gene expression data (no 3′ bias) for over 28,000 genes (GeneChip Mouse Gene ST 1.0 arrays; Affymetrix, Santa Clara, CA). We used the Robust Multichip Average (RMA) Express method (http://rmaexpress.bmbolstad.com/ written by Ben Bolstad, University of California, Berkeley, and provided in the public domain) to measure differential gene and probe level expression measures ($\log_2$), with a false-discovery rate (FDR) set at 5%. Quality control plots and summary measures were generated with R/Bioconductor 2.9.10.[23,24] Gene level measures were analyzed by using analysis of variance (ANOVA) models for repeated measures, considering temporal or regional effects, using custom scripts (written for SAS ver. 9.2; SAS, Cary, NC). Genes with $P < 0.01$ from the ANOVA models and a $\log_2$-fold change >2.5 were considered to be differentially expressed. Differentially expressed genes were analyzed for overlap with known networks, by using pathway analysis tools (GeneGo; St. Joseph, MI). Network significance was evaluated on the basis of the size of the intersection between our list of significantly differentially expressed genes and the set of genes/proteins corresponding to a network module/pathway. Each network was associated with a *z*-score that ranked the networks according to saturation with the objects from the experimental gene list. The *z*-score ranked the networks of the analyzed network algorithm with regard to their saturation with genes from the experiment. A high *z*-score means that the network is highly saturated with genes from the particular experiment. Each network was also associated with a *g*-score, which modifies the *z*-score on the basis of the number of canonical pathways used to build the network. If a network has a high *g*-score, it is saturated with expressed genes (from the *z*-score), and it contains many canonical pathways. A *P* value was determined by comparing the observed amount of intersection with the amount expected under the null hypothesis that the amount of overlap follows a hypergeometric distribution.

Results

A total of 28,000 genes were assessed over the three different time points in the five regions. Significant temporal differences in gene expression were found between 12-, 16-, and 20-week $LH_{BETA}T_{AG}$ RB tumors ($P < 10^{-8}$, two-way analysis of variance, ANOVA). In addition, analysis identified genes with a greater than 2.5-fold difference in expression between the three time points that varied depending on region. There were significant differences in gene expression across time for 190 genes apically, 84 genes anterolaterally, 126 genes posteriorly, 56 genes centrally, and 134 genes at the base (Tables 1A, 1B).

To identify functional activity of the unique genes, we performed pathway analysis (GeneGo software). Tables 2 to 6 show the key networks involved in cellular growth and proliferation, hypoxia, cell signaling, and angiogenesis for the five regions with key objects, processes, pathways, and statistical significance.

The basal regions (Table 2) of the RB tumors had significant differences ($P = 1.54 \times 10^{-11}$ to 3.72×10^{-61}) in regulation of Ras/G-protein signaling, regulation of cellular proliferation, mTOR/PKC signaling, and JAK/STAT signaling. The *z*-scores ranged from 13.56 to 48.21, and the *g*-scores ranged from 28.06 to 146.23. On analysis of networks, key elements mediating cellular proliferation included c-Myc, JAK/STAT, TGF-β, MDM2, RB protein, AMPK, let-7a microRNA, and p53. We also found cellular responses mediated by the PI3K/akt/mTOR pathway, as well as HIF, VEGF, NOTCH, and IGF-1 (Fig. 1).

The central regions (Table 3) of the tumors had significant differences ($P = 4.44 \times 10^{-7}$ to 3.22×10^{-61}) in regulation of cellular proliferation, response to oxygen levels, and regulation of oxidoreductase activity, JAK/STAT signaling, and regulation of cellular metabolism. The *z*-scores ranged from 8.81 to 45.46, and the *g*-scores ranged from 33.60 to 133.81. Network analysis showed that cellular proliferation and regulation were mediated by TNF-α, ERK1/2, RB protein, MAPK, VEGF, ubiquitin, TGF-β, and MDM2. Tumor response to oxygen levels was mediated by MMP-2 and -9, TGF-β, E-cadherin, c-Myc, PAI, VEGF, and CDK2/CDK4. In addition, the cellular proliferation

TABLE 1. Differential Gene Expression by More Than 2.5-Fold in Five Tumor Regions with the Corresponding Ratio of Change

A. Upregulated Genes

Base		Center		Apex		Anterior-lateral		Posterior-lateral	
Gene	Ratio of Change	Gene	Ratio of Change	Gene	Ratio of Change	Gene	Ratio of Change	Gene	Ratio of Change
KRT15	5.1448	*GM9912*	2.6366	*CENPK*	4.0012	*KRT16*	3.802	No gene name	3.6121
KRT4	5.0582			*2810417H13R1*	3.8653	No gene name	3.1226	*GEN1*	3.3636
CYP4A12B	4.6897			*CASC5*	3.7474	*SPINK5*	3.0778	*CCNB1*	3.2991
KRT13	4.5248			*BUB1*	3.7178	*XIST*	3.0497	*HMMR*	3.2884
KRT14	4.4163			*RRM2*	3.6037	*KRT14*	2.9956	*CCNB1*	3.2238
ANXA8	4.3149			*CDH9*	3.5187	*S100A9*	2.9409	*EG665955*	3.2117
KRT5	4.301			*MKI67*	3.5062	No gene name	2.9264	*CCNB1*	3.1662
TACSTD2	4.182			*PBK*	3.4692	*KRT5*	2.8168	*NCAPG2*	3.0262
KRT6B	4.1757			*KRT4*	3.466	*BC100530*	2.7341	*LCN2*	3.0002
CEACAM1	4.1426			*MCM6*	3.4537	*SNORD116*	2.7022	*LPHN2*	2.951
9930032O22RI	4.1396			*KRT14*	3.4365	No gene name	2.702	*C79407*	2.9377
UPK1B	4.0946			*NUDT10*	3.4343	*DSG3*	2.7003	*CRYBA1*	2.9014
DSG3	3.956			*GEN1*	3.3905	*SNORD116*	2.6892	*PTPN3*	2.8936
ENPP3	3.933			*CCNB1*	3.388	*MMP3*	2.6707	*CDH9*	2.8539
KRT6A	3.9257			*FAM111A*	3.3757	*SNORD116*	2.6558	*SHCBP1*	2.852
SLC6A14	3.8995			*CCNB1*	3.3655	*S100A8*	2.6524	*BUB1*	2.804
CBR2	3.8739			*KIF11*	3.3435	*CRYBA1*	2.628	*PBK*	2.7594
TMPRSS11B	3.7424			*CCNB1*	3.3391	*SNORD116*	2.5994	*6720489N17RI*	2.7205
DSC3	3.7068			*KRT6B*	3.3143	*GM9912*	2.5633	*GINS1*	2.7187
TRIM29	3.7054			*KRT15*	3.3032	*KRT6B*	2.5615	*CASC5*	2.6874
SCEL	3.6572			*TOP2A*	3.2889	*SCG3*	2.5175	*TTK*	2.6598
TMPRSS11A	3.6417			*CENPH*	3.2249	No gene name	2.5092	*SERPINA3N*	2.6336
ADH7	3.6356			*ANLN*	3.2177	*SNORD116*	2.5034	*TPX2*	2.629
ALDH3A1	3.6319			*HIST1H2AB*	3.1439			*LPHN2*	2.6035
AKR1B7	3.5832			*BC100530*	3.1268			*SGOL2*	2.5912
BC100530	3.5756			*C330027C09RI*	3.0901			*KIF4*	2.585
DSG1A	3.5619			*SGOL2*	3.074			*C330027C09R1*	2.5798
DSC2	3.5213			*KRT5*	3.0701			*PPIL5*	2.5518
PGLYRP1	3.4777			*CKS2*	3.0693			*KIF14*	2.5517
FABP6	3.4499			*MNS1*	3.0536			*CENPK*	2.5336
PLAC8	3.4191			*KRT13*	3.0486			*RRM2*	2.5299
DSP	3.3436			*ACTC1*	3.0294			*CHEK1*	2.528
S100A14	3.2942			*KIF4*	3.0204			*SNORD116*	2.5238
ADH1	3.2901			*NCAPG*	3.0026			*KIF2C*	2.5138
MUC4	3.2862			*SPC24*	3.0014			*CLSPN*	2.5114
RBP2	3.2579			*HELLS*	2.9981			*NUF2*	2.5102
CALML3	3.2514			*NUF2*	2.9795				
CAPG	3.2201			*KRT16*	2.965			*KIF14*	2.5517
KRT19	3.1758			*DSCC1*	2.9644			*CENPK*	2.5336
LUM	3.1756			*ARHGAP11A*	2.9578			*RRM2*	2.5299
CMAH	3.1643			*SMC2*	2.9405			*CHEK1*	2.528
SERPINB5	3.1593			*C79407*	2.9212			*SNORD116*	2.5238
EMP1	3.1549			*PRR11*	2.8937			*KIF2C*	2.5138
PPL	3.1142			*NDC80*	2.8826			*CLSPN*	2.5114
PYHIN1	3.09			*KRT6A*	2.8734			*NUF2*	2.5102
IL1F9	3.0649			*BIRC5*	2.8706			*KIF2C*	2.5138
DEFB1	3.0552			*LPHN2*	2.8672			*CLSPN*	2.5114
SAMD9L	3			*GINS1*	2.8565			*NUF2*	2.5102
FGFBP1	2.9933			*DSG3*	2.8543			*CLSPN*	2.5114
ANXA2	2.9889			*2810417H13RI*	2.8429			*NUF2*	2.5102
9930023K05RI	2.9783			*SHCBP1*	2.8422			*CLSPN*	2.5114
IFITM1	2.9492			*CKS2*	2.8379			*NUF2*	2.5102
GSTA3	2.9068			*CDC2A*	2.8331			*CLSPN*	2.5114
GPR110	2.9005			*LPHN2*	2.8233			*NUF2*	2.5102
DCN	2.847			*MASTL*	2.8215				
SPINK5	2.823			*TPX2*	2.8144				
EHF	2.7891			*KIF23*	2.8003				
KRT7	2.7817			*GM9912*	2.8001				
1600029D21RI	2.769			*TTK*	2.7778				
MALL	2.736			*CKS2*	2.7633				
S100A9	2.7304			*FBXO5*	2.7586				
OCM	2.7168			*EG665955*	2.7554				
CLDN7	2.6877			*PEG10*	2.7433				
				SPINK5	2.7412				

(*continues*)

TABLE 1 (*continued*). Differential Gene Expression by More Than 2.5-Fold in Five Tumor Regions with the Corresponding Ratio of Change

Base		Center		Apex		Anterior-lateral		Posterior-lateral	
Gene	Ratio of Change	Gene	Ratio of Change	Gene	Ratio of Change	Gene	Ratio of Change	Gene	Ratio of Change
GM9573	2.6769			*NCAPH*	2.7266				
PERP	2.6515			*KRT24*	2.7084				
ESRP1	2.6479			*ECT2*	2.695				
GSTO1	2.6415			*PPIL5*	2.6805				
GDA	2.6149			*RBBP8*	2.6706				
PTGR1	2.6138			*ANXA1*	2.67				
CYP2F2	2.6113			*CENPF*	2.6546				
IFITM1	2.5923			*CKAP2L*	2.6376				
C130090K23RI	2.5153			*CYP4A12B*	2.6161				
GALNT3	2.5097			*NCAPG2*	2.5946				
GM11428	2.5001			*DLGAP5*	2.5916				
				LYZ2	2.588				
				PRIM1	2.5849				
				DBF4	2.5832				
				LPHN2	2.5785				
				ATAD2	2.5765				
				TRIM59	2.5672				
				MCM3	2.5618				
				HMMR	2.5427				
				NFIA	2.5368				
				E2F8	2.534				
				EXO1	2.5174				
				2610039C10RI	2.5138				

B. Downregulated Genes

Base		Center		Apex		Anterior-lateral		Posterior-lateral	
Gene	Ratio of Change	Gene	Ratio of Change	Gene	Ratio of Change	Gene	Ratio of Change	Gene	Ratio of Change
CNGA1	−4.4701	*GUCY2F*	−4.1373	*PDE6B*	−5.0352	*CNGA1*	−4.6794	*OPN1SW*	−5.0585
RP1	−4.4608	*PDE6B*	−4.0316	*CNGA1*	−5.0191	*RCVRN*	−4.4971	*GUCY2F*	−4.6778
RCVRN	−4.3932	*RCVRN*	−3.8163	*RCVRN*	−4.8462	*PDE6B*	−4.4931	*RCVRN*	−4.5381
PDE6B	−4.3062	*RHO*	−3.7673	*RPE65*	−4.8052	*RHO*	−4.0053	*CNGA1*	−4.4204
GUCY2F	−3.9616	*2610034M16R1*	−3.7485	*PDE6A*	−4.7065	*RHO*	−3.9785	*PDE6B*	−4.3056
PDE6A	−3.9498	*RP1*	−3.5564	*RP1*	−4.6844	*RP1*	−3.9687	No gene name	−4.1752
RS1	−3.8567	*PDE6A*	−3.5066	*RHO*	−4.6441	*PDE6A*	−3.8735	*RP1*	−4.0818
RHO	−3.79	*CNGA1*	−3.4836	*GUCY2F*	−4.6367	*GNAT1*	−3.7975	*2610034M16RI*	−4.0801
TULP1	−3.6546	*REEP6*	−3.4382	*RDH12*	−4.5129	*RS1*	−3.6846	*PDE6A*	−4.0469
GRK1	−3.5238	*RS1*	−3.3294	*GNAT1*	−4.4516	*SAG*	−3.6444	*RHO*	−3.9724
RDH12	−3.4964	*SLC24A1*	−3.2645	*VTN*	−4.3343	*GUCY2F*	−3.638	*GRK1*	−3.8474
OPN1SW	−3.4265	*RPE65*	−3.2339	*GUCA1A*	−4.2548	*VTN*	−3.5997	*RHO*	−3.7115
GUCA1B	−3.4165	*ARR3*	−3.2278	*SAG*	−4.1852	*SLC24A1*	−3.449	*CDS1*	−3.6255
ADAMTS3	−3.4098	*VTN*	−3.1777	*RHO*	−4.1269	*2610034M16RI*	−3.4238	*RS1*	−3.5685
2610034M16RI	−3.3635	*TULP1*	−3.0543	*TTR*	−4.0968	*IMPGI*	−3.4029	*RDH12*	−3.5593
IMPG2	−3.3173	*GUCA1B*	−3.041	*TULP1*	−4.0863	*REEP6*	−3.4	*GUCA1B*	−3.4517
GM626	−3.3102	*IMPG1*	−3.0188	*GUCA1B*	−4.013	*GRK1*	−3.1713	*IMPG1*	−3.4482
PRPH2	−3.2885	*PDE6G*	−2.9703	*PDC*	−4.0107	*GUCA1B*	−3.1536	*ARR3*	−3.4129
SAG	−3.2643	*OPNIMW*	−2.9658	*2610034M16RI*	−4.0039	*GUCA1A*	−3.1167	*FABP12*	−3.3855
CALB1	−3.2542	*CNGB1*	−2.9629	*SLC24AI*	−3.9651	*PDC*	−3.0939	*C030002C11RI*	−3.3297
IMPG1	−3.2524	*GRK1*	−2.9333	*IMPG1*	−3.9048	*TULP1*	−3.0184	*SLC24A1*	−3.3201
PDE6G	−3.231	*ME1*	−2.9195	*RGR*	−3.8508	*PRPH2*	−3.0106	*REEP6*	−3.3172
WDR17	−3.2248	*CALB1*	−2.8971	*REEP6*	−3.8455	*CNGB1*	−2.9766	*VTN*	−3.3057
GNAT1	−3.2196	*NRL*	−2.8711	*GM626*	−3.8261	*OPN1MW*	−2.9231	*SAG*	−3.2897
RHO	−3.1948	*SAG*	−2.8696	*RS1*	−3.7915	*PDE6G*	−2.8083	*ADAMTS3*	−3.1062
SLC24A1	−3.188	*ABCA4*	−2.8646	*OPN1SW*	−3.7847	*RPE65*	−2.7849	*WDR17*	−3.0986
VTN	−3.1816	*PRPH2*	−2.8531	*IMPG2*	−3.7759	*ABCA4*	−2.7098	*TULP1*	−3.0714
FABP12	−3.1415	*C030002C11RI*	−2.8371	*GRK1*	−3.7481	*NR2E3*	−2.6847	*UPK1B*	−3.0451
ARR3	−3.0916	*RDH12*	−2.835	*CDS1*	−3.6674	*FABP12*	−2.6803	*CNGB1*	−3.0442
PDC	−3.0772	*GLBIL2*	−2.8234	*PRPH2*	−3.6533	*PROM1*	−2.652	*OPN1MW*	−3.0287
ROM1	−2.9229	*PEX5L*	−2.8231	*ROM1*	−3.6231	*IMPG2*	−2.6508	*FAM161A*	−3.0234
FAM161A	−2.9159	*WDR78*	−2.8094	*FABP12*	−3.6175	*GM626*	−2.6288	*GLB1L2*	−3.0131
A930003A15RI	−2.9133	*NXNL1*	−2.8054	*PDE6G*	−3.4549	*GM10664*	−2.61	*PDC*	−2.9972

(*continues*)

TABLE 1 (*continued*). Differential Gene Expression by More Than 2.5-Fold in Five Tumor Regions with the Corresponding Ratio of Change

Base		Center		Apex		Anterior-lateral		Posterior-lateral	
Gene	Ratio of Change	Gene	Ratio of Change	Gene	Ratio of Change	Gene	Ratio of Change	Gene	Ratio of Change
WDR78	−2.9098	*WDR17*	−2.7996	*ABCA4*	−3.4477	*NRL*	−2.6025	*TAC1*	−2.9925
GM10664	−2.8845	*NR2E3*	−2.7562	*PROM1*	−3.3796	*WDR17*	−2.5942	*ABCA4*	−2.988
SAMD7	−2.8688	*RGR*	−2.7358	*WDR78*	−3.3315	*GLB1L2*	−2.5708	*LRIT2*	−2.9737
ADAMTS3	−2.8323	*PROM1*	−2.7204	*CALB2*	−3.2487	*RDH12*	−2.5568	*PROM1*	−2.9684
OPN1MW	−2.8125	*SPATA1*	−2.7178	*GLB1L2*	−3.2272	*C530030P08RI*	−2.5517	*PDE6G*	−2.9669
REEP6	−2.7962	*RHO*	−2.7129	*NR2E3*	−3.2055	*WDR78*	−2.5363	*KRT12*	−2.9552
LRIT2	−2.7883	*PLA2R1*	−2.7107	*PPARGC1A*	−3.2005	No gene name	−2.5165	*PRPH2*	−2.9497
GUCA1A	−2.7699	*GNAT1*	−2.701	*CNGB1*	−3.1234	*LRIT2*	−2.5045	*WDR78*	−2.9474
ABCA4	−2.7201	*CDS1*	−2.6796	*MPP4*	−3.104			*GNAT1*	−2.9465
C030002C11RI	−2.7019	*FAM161A*	−2.6649	*WDR17*	−3.1008			*PSCA*	−2.946
CNGB1	−2.6999	*FABP12*	−2.6637	*NRN1*	−3.0902			*RPE65*	−2.9378
LRRC2	−2.6992	*LRIT2*	−2.6099	*NRL*	−3.0787			*PLA2R1*	−2.9029
SPATA1	−2.6869	*ME1*	−2.5699	*CALB1*	−3.077			*CDR2*	−2.9013
GM626	−2.665	*A930003A15RI*	−2.5299	*PEX5L*	−3.0711			*NRL*	−2.9007
HIST2H3C2	−2.6462	*3632451O06RI*	−2.5294	*GM11744*	−3.0574			*MPP4*	−2.8886
A330023F24RI	−2.6434	*BST1*	−2.5082	*LGI1*	−2.993			*GM626*	−2.874
PEX5L	−2.6154	*GM11744*	−2.5007	*FAM161A*	−2.9842			*GM11744*	−2.8575
PDE6C	−2.6118			*GM10664*	−2.9635			*RABGEF1*	−2.8558
TAC1	−2.5092			*CHRNB3*	−2.9436			*TDRD7*	−2.8429
				SLC17A6	−2.9268			*PEX5L*	−2.8263
				OPN1MW	−2.9101			*UNC13C*	−2.7611
				LRIT2	−2.9017			*NR2E3*	−2.7492
				COX8B	−2.8988			*APBH*	−2.7348
				ENPP2	−2.8935			*HERC3*	−2.7337
				ARR3	−2.8684			*PDE6C*	−2.7175
				HERC3	−2.8628			*GP2*	−2.7166
				C030002C11RI	−2.8626			*4833423E24RI*	−2.7154
				GM626	−2.8602			*DCN*	−2.7131
				CD59A	−2.8517			*CENPH*	2.7061
				SPATA1	−2.809			*RGR*	−2.7039
				ALDOC	−2.8089			*CALML3*	−2.6967
				LDHB	−2.7821			*STFA3*	−2.684
				SAMD7	−2.7803			*GUCA1A*	−2.6827
				GM626	−2.7474			*PPEF2*	−2.6757
				UNC13B	−2.7459			*NT5E*	−2.667
				RLBP1	−2.726			*NXNL1*	−2.6568
				RGS9	−2.7235			*IMPG2*	−2.6363
				RP1L1	−2.7206			*MLANA*	−2.6293
				GNB1	−2.7097			*PGLYRP1*	−2.6228
				PLA2G5	−2.7038			*C130021120RI*	−2.619
				PLA2R1	−2.674			*GM626*	−2.6093
				ME1	−2.664			*ATP8A2*	−2.6083
				KRT18	−2.6561			*S100A14*	−2.6036
				TAC1	−2.6465			*GM10664*	−2.6028
				CLIC6	−2.6461			*CALB2*	−2.6025
				PPEF2	−2.644			*CHRNB3*	−2.5758
				ATP8A2	−2.6388			*TYRP1*	−2.5606
				HK2	−2.638			*LRAT*	−2.5599
				LRRC67	−2.6246			*ADH1*	−2.5317
				GRIA3	−2.6234			*ROM1*	−2.5257
				ZDHHC2	−2.5984			*CSMD3*	−2.5134
				LYNX1	−2.5834			*PVALB*	−2.5085
				PVALB	−2.5725				
				GM626	−2.561				
				NXNL1	−2.5568				
				AIPL1	−2.5277				
				LRAT	−2.5118				
				ME1	−2.5094				
				CDR2	−2.5021				

and signaling pathways were mediated by JAK/STAT, ERK1/2, cyclin D1, and 14-3-3.

The apical regions (Table 4) of the tumors had significant differences ($P = 1.91 \times 10^{-7}$ to 1.29×10^{-83}) in PKA/G-protein signaling, regulation of cell proliferation, oxygen transport, and regulation of stress responses. The *z*-scores ranged from 9.40 to 57.83, and the *g*-scores ranged from 32.46 to 184.4. Tumor anatomic and morphogenic responses were found to be mediated by key elements, including VEGF, MMP-2, MMP-9, and TGF-β (Fig. 2, left). Cellular proliferation was found to be mediated by JAK/STAT, ERK1/2, c-Myc, NF-κB, IGF-1, TNF-α, and caspase-8. Finally, cellular responses to stress

TABLE 2. Key Networks with Associated Key Objects and Processes for Basal Tumor Regions

Top Networks	Key Network Objects	GO Processes	Total Nodes	Root Nodes	Pathways	*P*	*z*-Score	*g*-Score
3	STAT1, c-Raf-1, DNM1L (DRP1), NDPK B, 14-3-3 zeta/ delta	Regulation of cell proliferation, Positive regulation of cellular process, regulation of apoptosis	50	18	23	3.46×10^{-22}	22.44	51.19
4	mTOR, PKC, Tuberin, DLL1, NEURL1	Enzyme linked receptor protein signaling pathway, insulin-like growth factor receptor signaling pathway, cellular response to insulin stimulus	50	11	30	1.54×10^{-11}	13.56	51.06

were found to be mediated by HIF-1, NF-κB, and c-Myc (Fig. 2, right).

The anterior-lateral regions (Table 5) of the tumors had significant differences ($P = 1.41 \times 10^{-15}$ to 2.26×10^{-86}) in cellular proliferation, cytokine-mediated signaling pathways, leukocyte migration, and glycosaminoglycan biosynthetic processes. The *z*-scores ranged from 16.94 to 58.76, and the *g*-scores ranged from 34.63 to 58.76. Tumor signaling cascades and growth regulation were found to be mediated by TGF-β, MMP-2, MMP-9, fibronectin, c-Myc, and NF-κB. Cytokine-mediated signaling was found to involve TNF-α, NF-κB, ICAM, E-selectin, and CCL-2/CCL-3.

Finally, the posterior-lateral regions (Table 6) of the RB tumors had significant differences ($P = 1.07 \times 10^{-8}$ to 1.27×10^{-72}) in regulation of cellular proliferation, JAK/STAT signaling, and cytokine-mediated signaling. Network analysis showed anatomic morphogenesis and growth regulation to be mediated by TGF-β, MMP-2, MMP-9, ERK-1/2, MAPK, Akt, and VEGF. Cell proliferation and regulation of cellular processes were found to be mediated by TNF-α, ERK-1/2, VEGF, EGFR, MAPK, PKC, IGF-1, and COX-2.

DISCUSSION

In the present study, we identified genes that are differentially expressed in the $LH_{BETA}T_{AG}$ murine model of RB in five tumor regions (base, center, apex, anterior-lateral margin, posterior-

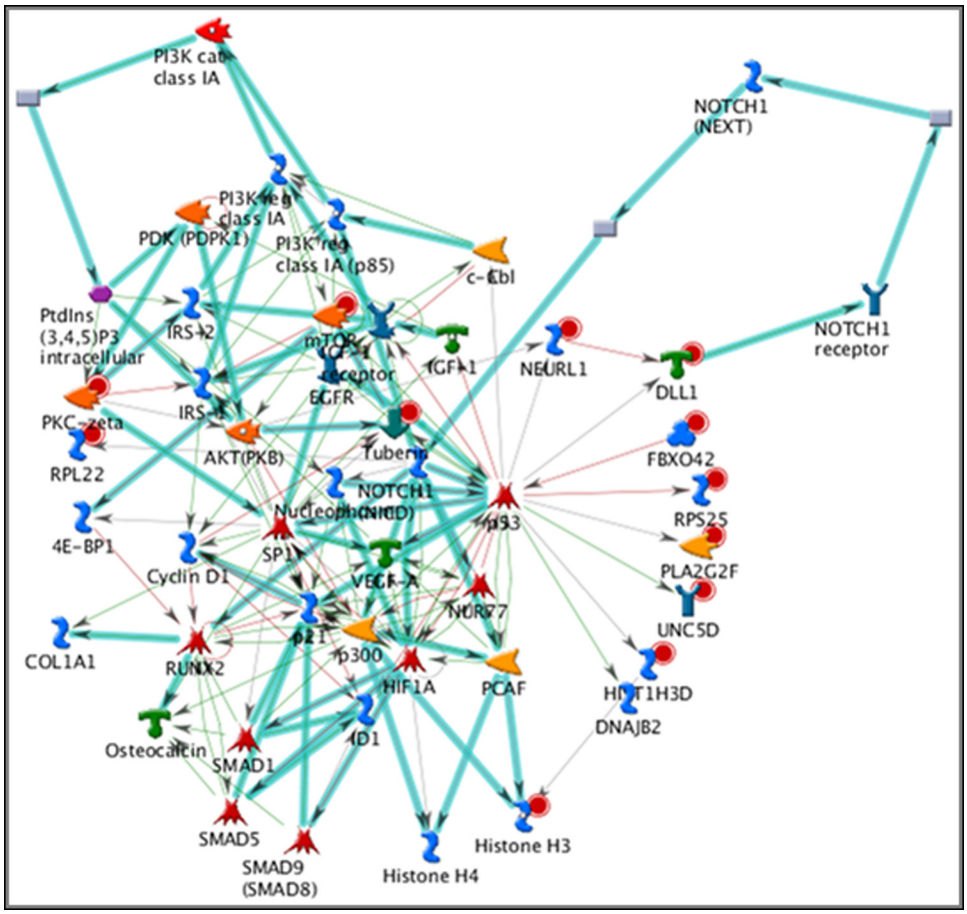

FIGURE 1. Network in basal aspects of tumors involved in hypoxic responses (network 4; $P < 10^{-11}$, 30 pathways), with key elements including mammalian target of rapamycin (mTOR), phosphoinositide-3 kinase (PI3K), Akt or protein ki), hypoxia-inducible factor (HIF), vascular endothelial growth factor (VEGF), NOTCH, and insulin-like growth factor (IGF-1). *Cyan lines*: fragments of canonical pathways; *red circles*: upregulated genes; *blue circles*: downregulated genes.

TABLE 3. Key Networks with Associated Key Objects and Processes for Central Tumor Regions

Top Networks	Key Network Objects	GO Processes	Total Nodes	Root Nodes	Pathways	*P*	*z*-Score	*g*-Score
2	*c-Raf-1, NCOA3, (pCIP/SRC3), H-Ras, NCOA2 (GRIP1/TIF2), TFF1*	Regulation of cell proliferation, positive regulation of cellular process	51	11	85	1.05×10^{-10}	12.29	118.54
5	*SMAD2, NF-κB, SMURF2, SerRS, RPS25*	Anatomic structure morphogenesis, response to oxygen levels	50	14	35	5.58×10^{-15}	16.04	59.79
9	*FOXO3A, 14-3-3 zeta/delta,* Cyclin D2, *GPIAP1, BTF*	JAK-STAT cascade involved in growth hormone signaling pathway, regulation of cell proliferation	50	20	12	4.22×10^{-25}	24.06	39.06

lateral margin), and at three time points in tumor development (12, 16, and 20 weeks). Overall, gene expression was shown to significantly differ temporally ($P < 10^{-8}$), as well as regionally. Of the 28,000 gene probe sets analyzed, we found differential expression of 190 genes apically, 84 genes anterolaterally, 126 genes posteriorly, 56 genes centrally, and 134 genes at the base. Analysis showed that these dysregulated genes were associated with multiple networks and canonical pathways, including regulation of cellular proliferation, cellular signaling and stress responses, response to hypoxia, angiogenesis, as well as anatomic morphogenesis and growth regulation.

As tumors grow, the proliferating cells experience an imbalance of oxygen metabolism, leading to a disorganized and irregular microvasculature network. As a result, there is reduced oxygen delivery, leading to a microenvironment with low oxygen partial pressure.[15,25–27] In the harsh tumor microenvironment depleted of oxygen and nutrients, cells undergo a hypoxic and/or angiogenic switch to support further growth. Growth of immature neovessels is stimulated, along with cell adaptation to hypoxia, including increase in glycolysis for energy metabolism.[26] These events represent a key transition in tumorigenesis as cells adapt, altering the gene expression necessary to drive further tumor proliferation.

We have previously shown that the tumor vasculature is highly heterogenous, with higher concentrations of large, mature vessels toward the base/center and smaller neovessels radiating into the periphery. These observations in both human and the $LH_{BETA}T_{AG}$ model suggest that RB tumors proliferate radially from the center.[20,22] The present study is the first to show the regional variation in gene expression by microarray in the $LH_{BETA}T_{AG}$ RB model. Gene expression was found to be dysregulated in a regional distribution, with the apex and base showing the most variation. We hypothesized that the apical areas correspond with the leading edges of the proliferating tumor consisting of highly metabolic, hyperproliferating cells, and neovessels dependent on growth factor support. Concurrently, the basal regions correspond to areas of hypoxic stress necessitating cellular adaptation. The current observations support our previous model of RB progression and blood vessel development, identifying potential canonical pathways that may mediate these responses in the transgenic model of RB tumors.[27–29]

In the apical regions, more advanced tumors had a significantly different expression of genes involved in cellular proliferation, hypoxia, angiogenesis, and regulation of stress responses. TGF-β, NF-κB, PTEN, and cyclin D2, as well as signaling through the JAK/STAT pathway were shown to be key mediators. TNF-α and caspase-8, which were found to be dysregulated in RB cell lines[30] and human RBs,[31] respectively, were also found in the present study to be dysregulated in advanced $LH_{BETA}T_{AG}$ tumors. Hypoxic responses, including angiogenesis, were also identified in the apical regions, areas of intense growth composed of hyperproliferating cells competing for oxygen and nutrients. These adaptations were mediated through hypoxia-inducible factor (HIF), vascular endothelial growth factor (VEGF), and matrix metalloproteinases (MMP-2 and -9), factors known to be significantly associated with advanced tumors with high degrees of hypoxia.

TABLE 4. Key Networks with Associated Key Objects and Processes for Apical Tumor Regions

Top Networks	Key Network Objects	GO Processes	Total Nodes	Root Nodes	Pathways	*P*	*z*-Score	*g*-Score
1	*TGF-β1, RUNX3,* TGF-β receptor type *II, GAS1, FALZ*	Organ development, anatomic structure morphogenesis, system development	50	8	140	1.91×10^{-7}	9.40	184.4
4	*NF-κB, FCGRT,* Cyclin D2, ISG20, SPT2	Positive regulation of cellular process, regulation of cell proliferation	50	14	27	1.21×10^{-15}	17.05	50.80
9	NF-κB, COX17, Nectin-2, PSMD7, LOC283412	Regulation of oxidoreductase activity, positive regulation of defense response, positive regulation of oxidoreductase activity, regulation of response to stress	50	27	4	1.34×10^{-40}	35.94	40.94

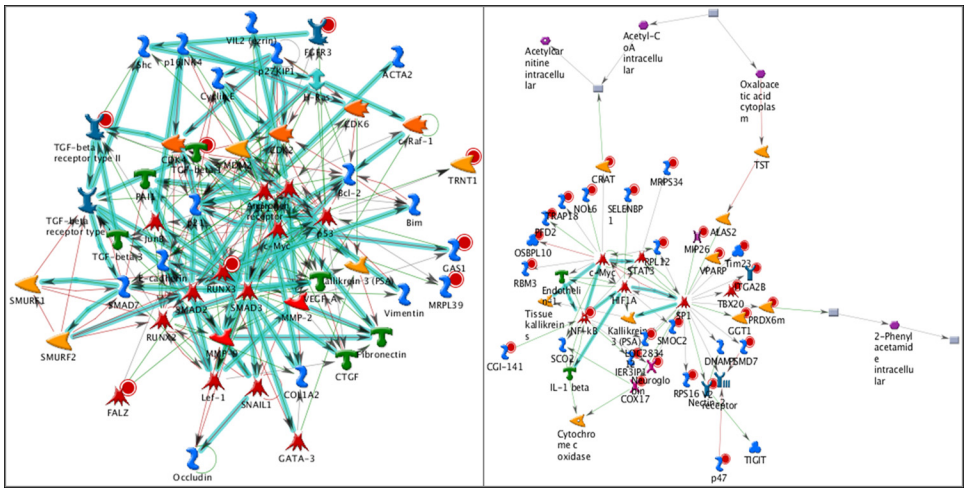

FIGURE 2. (**A**) Network involved in angiogenesis (network 1), in apical leading edges of tumors ($P < 10^{-7}$, 140 pathways). Key elements include vascular endothelial growth factor (VEGF), matrix metalloproteinase-9 (MMP-9), transforming growth factor-β (TGF-β). (**B**) Network involved in hypoxia (network 9) in the apical leading edges of tumors ($P < 10^{-40}$, 4 pathways). Response to hypoxia mediated by hypoxia-inducible factor (HIF).

The urokinase plasminogen activator (uPA) and the receptor (uPAR) may play an integral role in tumor proliferation and metastasis. The uPA system consists of serine proteases that lead to activation of plasmin, which in turn activates matrix metalloproteinases (MMPs). MMPs have been linked to tumor growth and metastasis for their role in the degradation of the extracellular matrix.[32] Recent studies have identified hypoxic elements within the genes that regulate the uPA system of several other tumors.[33,34] The present study has identified dysregulated genes involved in pathways for the uPA system as well as angiogenic pathways that use MMPs. These findings support our prior work showing enhanced tumor control with reduced expression of MMPs using anecortave acetate.[35] MMPs appear to play a key role in the tumor microenvironment, and studies are needed to further elucidate the mechanisms and effects of tumor treatment.

As neoplastic cells proliferate, they experience a highly anabolic state requiring altered function to provide sufficient energy and waste removal, thus preventing cell death signals.[36–38] In response to increasing metabolic demands, as well as altered microenvironments inside and outside the cells, neoplastic cells alter cellular metabolism, adopting a metabolic phenotype through differential gene expression for key enzymes and regulators of cellular metabolism.[39] Neoplastic cells preferentially use glycolysis, referred to as the Warburg effect, in normoxic and hypoxic conditions, rather than oxidative phosphorylation and its higher ATP yield. In basal regions, areas of RB tumors shown to consist of a high population of hypoxic cells, we found differential expression of genes involved in networks and pathways that are upstream regulators of tumor metabolism, including PI3K/Akt/mTOR, IGF-1 signaling, and AMPK. In addition, our study showed significant involvement of HIF and Akt, both of which have been shown to increase GLUT1, a glucose transport receptor.[37] Our prior studies in the $LH_{BETA}T_{AG}$ RB tumor model have demonstrated the efficacy of targeting cellular metabolism in enhancing tumor control. Using 2-DG, a glycolytic inhibitor, we have shown that tumor burden is significantly reduced when treated with both systemic and local subconjunctival delivery of 2-DG. We have also recently shown that local delivery of 2-DG, when combined with chemotherapy, further enhances tumor control over either treatment alone.[19]

In addition, similar to prior human RB microarray gene expression studies, the PI3K/Akt/mTOR pathway was found to be dysregulated, potentially implicating mTOR as a therapeutic target.[40] We found significant differential expression of this network in basal regions of advanced tumors, regions shown to experience significant hypoxia compared with other regions. The mammalian target of rapamycin (mTOR) is a serine-threonine kinase that is composed of two multiprotein complexes. Activation of these complexes leads to phosphorylation of downstream effectors, leading to regulation of protein translation, cell growth, proliferation, and metabolism.[41] Hypoxia has been shown to be a negative regulator of mTOR complexes, thus potentially acting as an inhibitor of growth and progression. However, it has been proposed that hypoxia drives the mutations necessary to deregulate mTOR signaling, termed hypoxic tolerance. As a result, it may be important for tumor cells to retain control of mTOR signaling for continued growth and proliferation.[18] mTOR inhibitors have been investigated in other tumors, and further studies are needed to define the role of mTOR and inhibitors of this pathway in RB tumor control. Notably, early studies with focal delivery of rapamycin in the $LH_{BETA}T_{AG}$ RB model show promise, as the mTOR inhibitor led

TABLE 5. Key Networks with Associated Key Objects and Processes for Anterolateral Tumor Regions

Top Networks	Key Network Objects	GO Processes	Total Nodes	Root Nodes	Pathways	*P*	*z*-Score	*g*-Score
5	*SMURF2, CRELD2, eIF4A1, SARA, SAHH2*	Response to organic cyclic substance, transforming growth factor beta receptor signaling pathway	50	14	24	1.41×10^{-15}	16.94	46.94
8	*CCL13, HMG1* (amphotericin), *NDPK B, HRPT2,* Symplekin	Translational elongation, leukocyte migration, cytokine-mediated signaling pathway, response to mechanical stimulus, translation	50	21	9	9.13×10^{-28}	26.67	37.92

TABLE 6. Key Networks with Associated Key Objects and Processes for Posterolateral Tumor Regions

Top Networks	Key Network Objects	GO Processes	Total Nodes	Root Nodes	Pathways	*P*	*z*-Score	*g*-Score
1	*SMAD1, SMAD2, TGFb 1, SCAP, RPS27A*	Anatomic structure morphogenesis, organ development, regulation of developmental process	50	11	67	2.42×10^{-11}	13.26	97.01
3	*SHP-2,* Ubiquitin, *IGF-2, NIX, GlyRS*	Regulation of cell proliferation, regulation of cellular process	50	9	38	1.07×10^{-8}	10.70	58.20

to enhanced tumor control (Murray TG, et al. *IOVS* 2010;43: ARVO E-Abstract 2067).

Our current and previous findings support an evolving and complex cellular metabolic phenotype that differs in early versus advanced tumors, as well as variations secondary to the local, heterogeneous tumor microenvironment. This study provides further evidence of dysregulation of pathways involved in cellular metabolism, including genes to assess at a functional level to determine the effect on tumor growth and development.

In addition, the study is the first to show temporal variation in gene expression with advanced tumors compared to earlier tumors examined with microarray analysis. In transgenic RB tumors, differential gene expression and associated pathways suggest potential mechanisms of tumorigenesis. These specific genes and pathways require further functional analysis to determine whether direct targeting has an effect on tumor growth and development, or whether the changes seen are indirect effects of other tumorigenic processes and would not serve as useful targets for tumor control. As with other tumors, we propose that regions of RB tumors have differential gene expression and may respond differently to various treatments, depending on the tumor's age, tumor burden, location, hypoxia, vasculature, and cellular metabolism. Therefore, the present study provides evidence of regional and temporal tumor heterogeneity, emphasizing the potential importance of timing in gene expression in the development of optimally timed, multimodal treatments with agents that target tumor cells, as well as components of the tumor microenvironment, including angiogenesis, hypoxia, and cellular metabolism. We propose that future treatment of RB tumors must target not only proliferating tumor cells, but also the local tumor microenvironment, in a multimodal, optimally timed, local approach.

As functional analyses are performed on specific genes and pathways, including studies on targeting key elements, it is important to identify alterations in gene expression after treatment as well as to identify key escape pathways that cells use during times of cellular stress. These escape pathways may prove to be important regarding resistance and adaptation of tumor cells to current and future targeted therapies.

Limitations of the present study include the small sample size of three mice at each time point (12, 16, and 20-weeks), as well as for each different region at each of these time points. In addition, we investigated the effects of time and location in the $LH_{BETA}T_{AG}$ murine model of RB, which has been shown to share many similarities with human RB, but the correlation in gene expression between human and mouse tumors has not been fully determined. As a result, before the current findings can be related to human RB, further functional studies are needed of transgenic RB tumors and human RB cell lines.

In conclusion, the findings in our study have shown that gene expression in the $LH_{BETA}T_{AG}$ model of RB has significant temporal variations. In addition, we have shown significant regional variations, with the apical and basal regions exhibiting dysregulation of genes in key pathways involved in the regulation of cellular proliferation and growth, response to oxygen levels and hypoxia, and regulation of cellular processes, cellular signaling cascades, and angiogenesis. Prior studies have defined the gene expression profiles of RB tumors[40,42]; our study of the $LH_{BETA}T_{AG}$ murine model suggests that these gene expression profiles may be dynamic, varying in a temporal and regionally dependent fashion. We anticipate that future developments in ocular oncology will focus on locally delivered, optimally timed therapies that target tumor cells as well as the tumor microenvironment.

References

1. Tamboli A, Podgor MJ, Horm JW. The incidence of retinoblastoma in the United States: 1974 through 1985. *Arch Ophthalmol.* 1990; 108:128–132.
2. Pendergrass TW, Davis S. Incidence of retinoblastoma in the United States. *Arch Ophthalmol.* 1980;98:1204–1210.
3. Abramson DH. Retinoblastoma incidence in the United States. *Arch Ophthalmol.* 1990;108:1514.
4. Devesa SS. The incidence of retinoblastoma. *Am J Ophthalmol.* 1975;80:263–265.
5. Abramson DH. Retinoblastoma in the 20th century: past success and future challenges. The Weisenfeld lecture. *Invest Ophthalmol Vis Sci.* 2005;46:2683–2691.
6. Benz MS, Scott IU, Murray TG, Kramer D, Toledano S. Complications of systemic chemotherapy as treatment of retinoblastoma. *Arch Ophthalmol.* 2000;118:577–578.
7. Chan HS, Gallie BL, Munier FL, Beck Popovic M. Chemotherapy for retinoblastoma. *Ophthalmol Clin North Am.* 2005;18:55–63, viii.
8. Gombos DS, Hungerford J, Abramson DH, et al. Secondary acute myelogenous leukemia in patients with retinoblastoma: is chemotherapy a factor? *Ophthalmology.* 2007;114:1378–1383.
9. Lin P, O'Brien JM. Frontiers in the management of retinoblastoma. *Am J Ophthalmol.* 2009;148:192–198.
10. Shields CL, Shields JA. Basic understanding of current classification and management of retinoblastoma. *Curr Opin Ophthalmol.* 2006; 17:228–234.
11. Schefler AC, Cicciarelli N, Feuer W, Toledano S, Murray TG. Macular retinoblastoma: evaluation of tumor control, local complications, and visual outcomes for eyes treated with chemotherapy and repetitive foveal laser ablation. *Ophthalmology.* 2007;114:162–169.
12. Knudson AG Jr. Mutation and cancer: statistical study of retinoblastoma. *Proc Natl Acad Sci U S A.* 1971;68:820–823.
13. Corson TW, Gallie BL. One hit, two hits, three hits, more?—genomic changes in the development of retinoblastoma. *Genes Chromosomes Cancer.* 2007;46:617–634.
14. Bissell MJ, Radisky DC, Rizki A, Weaver VM, Petersen OW. The organizing principle: microenvironmental influences in the normal and malignant breast. *Differentiation.* 2002;70:537–546.
15. Hanahan D, Weinberg RA. The hallmarks of cancer. *Cell.* 2000; 100:57–70.
16. Coussens LM, Werb Z. Inflammation and cancer. *Nature.* 2002; 420:860–867.
17. Dewhirst MW, Cao Y, Moeller B. Cycling hypoxia and free radicals regulate angiogenesis and radiotherapy response. *Nat Rev Cancer.* 2008;8:425–437.

18. Wouters BG, Koritzinsky M. Hypoxia signalling through mTOR and the unfolded protein response in cancer. *Nat Rev Cancer.* 2008; 8:851–864.
19. Boutrid H, Jockovich ME, Murray TG, et al. Targeting hypoxia, a novel treatment for advanced retinoblastoma. *Invest Ophthalmol Vis Sci.* 2008;49:2799–2805.
20. Pina Y, Boutrid H, Schefler A, et al. Blood vessel maturation in human and lhbetatag mouse model retinoblastoma tumors: spatial distribution of neovessels and mature vessels and its impact on ocular treatment. *Invest Ophthalmol Vis Sci.* 2009;50:1020–1024.
21. Windle JJ, Albert DM, O'Brien JM, et al. Retinoblastoma in transgenic mice. *Nature.* 1990;343:665–669.
22. Pina Y, Boutrid H, Schefler A, et al. Blood vessel maturation in retinoblastoma tumors: spatial distribution of neovessels and mature vessels and its impact on ocular treatment. *Invest Ophthalmol Vis Sci.* 2009;50:1020–1024.
23. Gentleman RC, Carey VJ, Bates DM, et al. Bioconductor: open software development for computational biology and bioinformatics. *Genome Biol.* 2004;5:R80.
24. Team RDC. *R: A Language and Environment for Statistical Computing*. R Foundation for Statistical Computing, Vienna, Austria; 2010.
25. Konerding MA, Miodonski AJ, Lametschwandtner A. Microvascular corrosion casting in the study of tumor vascularity: a review. *Scanning Microsc.* 1995;9:1233–1243, discussion 1243–1234.
26. Bergers G, Benjamin LE. Tumorigenesis and the angiogenic switch. *Nat Rev Cancer.* 2003;3:401–410.
27. Marine JC, Jochemsen AG. Mdmx and Mdm2: brothers in arms? *Cell Cycle.* 2004;3:900–904.
28. Laurie NA, Donovan SL, Shih CS, et al. Inactivation of the p53 pathway in retinoblastoma. *Nature.* 2006;444:61–66.
29. Calin GA, Croce CM. MicroRNAs and chromosomal abnormalities in cancer cells. *Oncogene.* 2006;25:6202–6210.
30. Mocellin S, Rossi CR, Pilati P, Nitti D. Tumor necrosis factor, cancer and anticancer therapy. *Cytokine Growth Factor Rev.* 2005;16:35–53.
31. Harada K, Toyooka S, Shivapurkar N, et al. Deregulation of caspase 8 and 10 expression in pediatric tumors and cell lines. *Cancer Res.* 2002;62:5897–5901.
32. Rademakers SE, Span PN, Kaanders JH, Sweep FC, van der Kogel AJ, Bussink J. Molecular aspects of tumour hypoxia. *Mol Oncol.* 2008;2:41–53.
33. Fink T, Kazlauskas A, Poellinger L, Ebbesen P, Zachar V. Identification of a tightly regulated hypoxia-response element in the promoter of human plasminogen activator inhibitor-1. *Blood.* 2002;99:2077–2083.
34. Schilling D, Bayer C, Geurts-Moespot A, et al. Induction of plasminogen activator inhibitor type-1 (PAI-1) by hypoxia and irradiation in human head and neck carcinoma cell lines. *BMC Cancer.* 2007;7:143.
35. Bajenaru ML, Pina Y, Murray TG, et al. Gelatinase expression in retinoblastoma: modulation of LH(BETA)T(AG) retinal tumor development by anecortave acetate. *Invest Ophthalmol Vis Sci.* 2010;51:2860–2864.
36. DeBerardinis RJ, Lum JJ, Hatzivassiliou G, Thompson CB. The biology of cancer: metabolic reprogramming fuels cell growth and proliferation. *Cell Metab.* 2008;7:11–20.
37. Tennant DA, Duran RV, Boulahbel H, Gottlieb E. Metabolic transformation in cancer. *Carcinogenesis.* 2009;30:1269–1280.
38. King A, Gottlieb E. Glucose metabolism and programmed cell death: an evolutionary and mechanistic perspective. *Curr Opin Cell Biol.* 2009;21:885–893.
39. Tennant DA, Duran RV, Gottlieb E. Targeting metabolic transformation for cancer therapy. *Nat Rev Cancer.* 2010;10:267–277.
40. Chakraborty S, Khare S, Dorairaj SK, Prabhakaran VC, Prakash DR, Kumar A. Identification of genes associated with tumorigenesis of retinoblastoma by microarray analysis. *Genomics.* 2007;90:344–353.
41. Meric-Bernstam F, Gonzalez-Angulo AM. Targeting the mTOR signaling network for cancer therapy. *J Clin Oncol.* 2009;27:2278–2287.
42. Ganguly A, Shields CL. Differential gene expression profile of retinoblastoma compared to normal retina. *Mol Vis.* 2010;16: 1292–1303.